Applied Catalysis B: Environmental 327 (2023) 122446

Contents lists available at ScienceDirect

Applied Catalysis B: Environmental

journal homepage: www.elsevier.com/locate/apcatb

In-situ growing nickel phthalocyanine supramolecular structure on carbon nanotubes for efficient electrochemical CO_2 conversion

Yucheng Jin, Xiaoning Zhan, Yingting Zheng, Hailong Wang *, Xiaolin Liu, Baoqiu Yu, Xu Ding, Tianyu Zheng, Kang Wang *, Dongdong Qi, Jianzhuang Jiang *

Beijing Advanced Innovation Center for Materials Genome Engineering, Beijing Key Laboratory for Science and Application of Functional Molecular and Crystalline Materials, Department of Chemistry, University of Science and Technology Beijing, Beijing 100083, China

ARTICLE INFO

Keywords:
Hydrogen-bonded organic ribbon
Nickel phthalocyanine
Carbon dioxide reduction reaction
Electrocatalysts

ABSTRACT

Heterogeneous catalysts made up of molecule-based catalysts on conductive substrates enable the large current density, high selectivity, and easy operation for carbon dioxide reduction reaction towards the practical use. Herein, we report a hydrogen-bonded supramolecular structure (**1**) assembled from asymmetric A_3B-type nickel phthalocyanine $NiPc(OH)_6(DCNFO)$, which is afforded via solvothermal reaction of 2,3,9,10,16,17,23,24-octahydroxyl-phthalocyaninato nickel with tetrafluoroterephthalene. Single crystal X-ray diffraction analysis reveals the one-dimensional supramolecular ribbons of **1** formed from individual modules via hydrogen-bond between the hydroxyl groups, showing good solution resistance due mainly to the additional strong π-π interactions. Nevertheless, in-situ growing **1** on carbon nanotubes generates a phthalocyanine-based composite for gas diffusion electrode, displaying the highly selective conversion of CO_2 to CO with Faradaic efficiency > 98% at a wide voltage range from − 0.5 to − 1.2 V versus reversible hydrogen electrode, a high current density of 353 mA cm^{-2} at − 1.2 V, and stable cycling at 150 mA cm^{-2} for 40 h in 0.5 M $KHCO_3$ electrolyte. Employment of 1.0 M KOH results in a further improved current density of 620 mA cm^{-2} at − 1.2 V and higher stable cycling current density of 230 mA cm^{-2} for 40 h.

1. Introduction

The conversion of carbon dioxide to valuable fuels and chemicals is an important link for carbon circulation in a sustainable economy [1–9]. The electrochemical carbon dioxide reduction reaction (CO_2RR) has attracted increasing research interests due to the source renewability of electricity power as well as the mild operational conditions [10–14]. In this direction, inorganic catalysts and metal complexes are two kinds of dominant electrochemical CO_2RR catalysts. The former species with fast electron transport nature and rich active sites are capable of delivering high current densities to electrochemically convert CO_2 molecules [10–12]. Compared with inorganic electrocatalysts, homogeneous metal complexes are particularly important systems for precious mechanistic studies at the molecular level [12,15–23], ensuring the superior selectivity and specific activity in the CO_2RR by tailoring the well-defined active site structures. Heterogenizing molecular catalysts is generally preferable for practical applications, as demonstrated by the recent research progress in immobilizing molecules on conductive supports to realize prominent catalytic performance [17–24]. Such heterogenization strategy enables the efficient electron transport to the catalytically active sites, dense spatial density of molecular complexes on electrodes, and operational convenience as well as improvement of stability and reusability. However, it is still an outstanding challenge to generate high current densities with high selectivity for molecule-based catalysts due possibly to their aggregation and low loading on conductive substrates.

Transition-metal tetrapyrroles such as metal porphyrins (MPor) and phthalocyanine (MPc) have been a kind of well-known metal complexes electrocatalysts for CO_2RR [25–29], with the first study of cobalt phthalocyanine (CoPc) for electrocatalytic CO_2 conversion initiated as early as in 1970s [30]. In the recent several years, MPor- and MPc-based electrocatalysts made up of molecular materials immobilized on conductive carbonaceous supports have sparked the renewed interests, because their superior heterogeneous electrocatalytic performances in water phase are comparable to some of the excellent metallic catalysts and metal-nitrogen-carbons [20,31–54]. In this regard, the excellent electrocatalytic activities of molecular metal phthalocyanines seriously

* Corresponding authors.
E-mail addresses: hlwang@ustb.edu.cn (H. Wang), kangwang@ustb.edu.cn (K. Wang), jianzhuang@ustb.edu.cn (J. Jiang).

https://doi.org/10.1016/j.apcatb.2023.122446
Received 2 December 2022; Received in revised form 16 January 2023; Accepted 8 February 2023
Available online 14 February 2023

depend on their well-dispersed form on conductive substances as well as the innovation of electrolyzer with fast gas diffusion instead the liquid mode in H-type cell [20,33,39]. For example, the CoPc molecules dispersed on carbon nanotubes (CNTs) have been demonstrated to exhibit high Faradaic efficiency (FE) and turnover frequency (TOF), but usually at low current densities < 40 mA cm^{-2} towards electrochemical CO_2 conversion using H-type cell [55–58]. In addition, the high cycling current densities over 150 mA cm^{-2} accompanying with favorable selectivity for CoPc molecular catalyst have been achieved by using a flow cell [39]. Until recently, the discovery of nickel phthalocyanine compound in a molecularly dispersed form on CNTs, displaying > 99.5% CO_2-to-CO selectivity at a high current density of 300 mA cm^{-2}, has distracted the research attention from CoPc catalysts to other metallic analogs [59–70]. It is worth noting that porous reticular materials provide another effective approach for molecular electrocatalysts heterogeneity by integrating catalytically active modules into metal−organic frameworks (MOFs) [3,36,37,48,71–73] and covalent organic frameworks (COFs) [6,42–47,74–78] with the help of coordination and covalent interactions, respectively. In contrast to molecular electrocatalysts, these molecule-based polymeric materials conventionally display the enhanced stability and high selectivity but still inferior current density due possibly to the inhomogeneous dispersion on conductive substances of grinding electrodes.

Herein, we introduce *in-situ* synthesis of nickel phthalocyanine supramolecular structure for **1** on CNTs to provide a **1**@CNT composite based on the solvothermal reaction of 2,3,9,10,16,17,23,24-octahydroxyl-phthalocyaninato nickel ($NiPc(OH)_8$) with tetrafluoroterephthalene (TFPN) in N,N-dimethylformamide (DMF). This supramolecular structure of **1** is assembled from an asymmetric A_3B-type nickel phthalocyanine molecule $NiPc(OH)_6$(DCNFO) through hydrogen-bond and π-π interactions, exhibiting insolubility and good solvent resistance. It therefore could be regarded as a supramolecular polymeric catalyst, different from those reported mononuclear metallic phthalocyanines molecules. **1**@CNT has been used as the gas diffusion electrode (GDE) towards CO_2RR in 0.5 M $KHCO_3$ electrolyte, showing outstanding CO_2-to-CO selectivity, as demonstrated by $FE_{CO} > 98\%$ at a wide voltage range from − 0.5 to − 1.2 V versus reversible hydrogen electrode (RHE). Moreover, the current density is able to reach 353 mA cm^{-2} at − 1.2 V, and the stable current density of 150 mA cm^{-2} has been cycled for 40 h. In particular, employment of 1.0 M KOH electrolyte leads to the current density up to 620 mA cm^{-2} at − 1.2 V as well as higher stable cycling current density of 230 mA cm^{-2} for 40 h. Theoretical calculations and experimental data disclose the increased electron density around nickel ion in $NiPc(OH)_6$(DCNFO) in comparison with that of $NiPc(OH)_8$ due to introduction of 3,6-dicyano-4,5-difluoro-1,2-phenylene-bisoxy group to the former compound. This, in combination with the thin-layered dispersion of **1** on CNTs, plays an important role in its excellent electrocatalytic performance.

2. Experimental

2.1. General remarks

All regents were commercially available and directly employed. The synthesis of $NiPc(OH)_8$ was referred to the previous literature procedure [71].

2.2. Preparation of 1

A Pyrex tube (9 × 6 mm, o.d. × i.d.) was filled with $NiPc(OH)_8$ (14.0 mg, 0.02 mmol), TFPN (8.0 mg, 0.04 mmol), and DMF (2.0 mL). After sonicating the tube for 15 min followed by flash freezing in a liquid N_2 bath, the frozen tube was degassed and slowly thawed to room temperature. Such an operation was repeated for three times, then the tube was sealed by flame with a length of ca. 18 cm. The reaction was performed at 120 °C for 3 days. The solid was isolated via centrifugation and successively washed with DMF and acetone for three times. The product was collected and dried under air overnight to provide black-green needle-like single crystals of **1** (8.5 mg) in a yield of 36.9%.

2.3. Preparation of 1@CNT(n)

1 @CNT(22.1) was selected as representative to illustrate the synthesis of these composites. A Pyrex tube (9 × 6 mm, o.d. × i.d.) was filled with $NiPc(OH)_8$ (14.0 mg, 0.02 mmol), tetrafluoroterephthalene (8.0 mg, 0.04 mmol), carbon nanotubes (CNTs, 30 mg), and DMF (2.0 mL). After sonicating the tube for 15 min followed by flash freezing in a liquid N_2 bath, the frozen tube was degassed and slowly thawed to room temperature. Such an operation was repeated for three times, the tube was sealed by flame with a length of ca. 18 cm. The reaction was performed at 120 °C for 3 days. The solid was isolated via centrifugation and successively washed with DMF and acetone for three times. The product was collected and dried at room temperature to give **1**@CNT (22.1). Following the same procedure, **1**@CNT(7.8), **1**@CNT(14.5), **1**@CNT(29.8), **1**@CNT (50.0), and **1**@CNT (75.0) were prepared by adding different amounts of CNTs, namely 100.0, 50.0, 20.0, 8.5, and 2.8 mg, respectively.

2.4. Preparation of 1&CB

A mixture of **1** (2.0 mg) and carbon black (CB, 7.1 mg) was grinded to obtain **1**&CB.

2.5. Preparation of 1&CNT

A mixture of **1** (2.0 mg) and CNTs (7.1 mg) was grinded to obtain **1**&CNT.

2.6. Preparation of $NiPc(OH)_8$@CNT

A Pyrex tube (9 × 6 mm, o.d. × i.d.) was filled with $NiPc(OH)_8$ (14.0 mg, 0.02 mmol), CNTs (30.0 mg), and DMF (2.0 mL). After sonicating the tube for 15 min followed by flash freezing in a liquid N_2 bath, the frozen tube was degassed and slowly thawed to room temperature. After such a process was repeated for three times, the tube was sealed by flame with a length of ca. 18 cm. The reaction was performed at 120 °C for 3 days. The solid was isolated via centrifugation and successively washed with DMF and acetone three times. The product was collected and dried at room temperature overnight to $NiPc(OH)_8$ @CNT as a control electrocatalyst.

3. Results and discussion

3.1. Crystal structure of 1

A new nickel phthalocyanine compound **1** was prepared through the solvothermal reaction of $NiPc(OH)_8$ with tetrafluoroterephthalene in DMF at 120 °C for 72 h (Scheme 1). After the reaction, black-green needle-like crystals of **1** were observed, and the structure of this

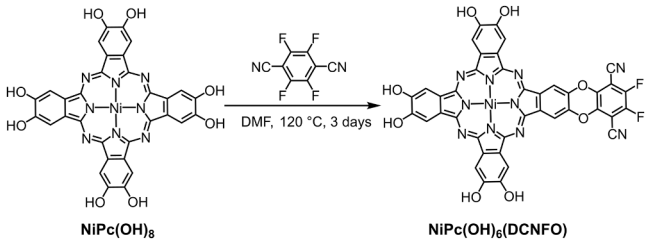

Scheme 1. Synthesis of $NiPc(OH)_6$(DCNFO) as building block for supramolecular compound **1**.

compound was solved by single crystal X-ray diffraction study. **1** subordinates to monoclinic system with space group $P2_1/n$ (Table S1). The definite structure of this compound is shown in Fig. 1a–c. Its molecular building block, NiPc(OH)$_6$(DCNFO), is made up of a 3,6-dicyano-4,5-difluoro-1,2-phenylene-bisoxy group connecting on the 2,3-positions of 9,10,16,17,23,24-hexahydroxyl-phthalocyaninato nickel segment (Fig. 1a), forming a new asymmetric A_3B-type nickel phthalocyanine molecule with C_{2v} symmetry. The center nickel ion is coordinated with four isoindoles nitrogen atoms, and the Ni-N bond lengths are in the range of 1.896(3)– 1.905(3) Å, which are comparable to the previous results of nickel phthalocyanine [79]. Each NiPc(OH)$_6$(DCNFO) molecule interacts with four DMF molecules through the hydrogen bonds between four different hydroxyl groups and amide oxygen atoms of DMF molecules (O1 −H1···O12#1, O3 −H3A···O9, O5 −H5···O10 and O6 −H6A···O11, symmetry code #1: -x, 1-y, 1-z) (Fig. 1a and Table S2). In addition, a NiPc(OH)$_6$(DCNFO) molecule is also linked by two neighboring phthalocyanine molecules via hydrogen bonds among hydroxyl groups (O2 −H2···O3#2 and O4 −H4···O2#3, symmetry code #2: −1/2 +x, 3/2-y, 1/2 +z and #3: 1/2 +x, 3/2-y, −1/2 +z), forming a zigzag supramolecular ribbons (Fig. 1b and Table S2). These zigzag supramolecular chains are packed through strong π-π interactions, as indicated by the short distance of 3.257 Å and 3.331 Å between neighboring macrocyclic N_4 planes (Fig. 1c).

3.2. Characterizations of bulk 1

The newly obtained compound **1** together with its two precursors, TFPN and NiPc(OH)$_8$, were characterized by Fourier transform infrared (FT-IR) spectroscopy (Fig. 1d). **1** has the characteristic absorption peak of cyano (C≡N) from TFPN at 2244 cm^{-1} and the signals of ether (C-O-C) at 1277 cm^{-1} and 1010 cm^{-1} [46], disclosing the covalent connection of two TFPN and NiPc(OH)$_8$ moieties. The UV–vis spectrum of NiPc(OH)$_8$ in DMF exhibits a strong Q band at 685 nm, Fig. 1e. In contrast, the Q band of **1** dispersed in DMF has a red shift to 695 nm with a broad adsorption, indicating the presence of *J*-aggregation form in this compound due to the strong intermolecular π-π interactions. This is consistent with the observed slide angles of 26.0° and 42.3° between different phthalocyanine dimers in the crystal structure of **1**, (Fig. S1). Furthermore, elemental analysis of **1** is slight deviated from the chemical composition made up of a phthalocyanine molecule with four crystallized DMF molecules due to the partial solvent loss at room temperature (Table S3). The bulk solid was performed on powder X-ray diffractometer, and the diffraction peaks are overall similar to the simulated data from the single crystal structure (Fig. 1f). Pawley refinement upon powder X-ray diffraction (PXRD) data displays $a = 7.3622(3)$ Å, $b = 33.0215(11)$ Å, $c = 20.8136(6)$ Å, $\alpha = \gamma = 90°$, and $\beta = 97.386(3)°$ with $R_p = 4.34\%$ and $R_{wp} = 5.49\%$. This, in combination with the elemental analytic results, confirms the bulk product purity. This compound is insoluble in common organic solvents including acetone, dichloromethane, methanol, and tetrahydrofuran, and has a tiny

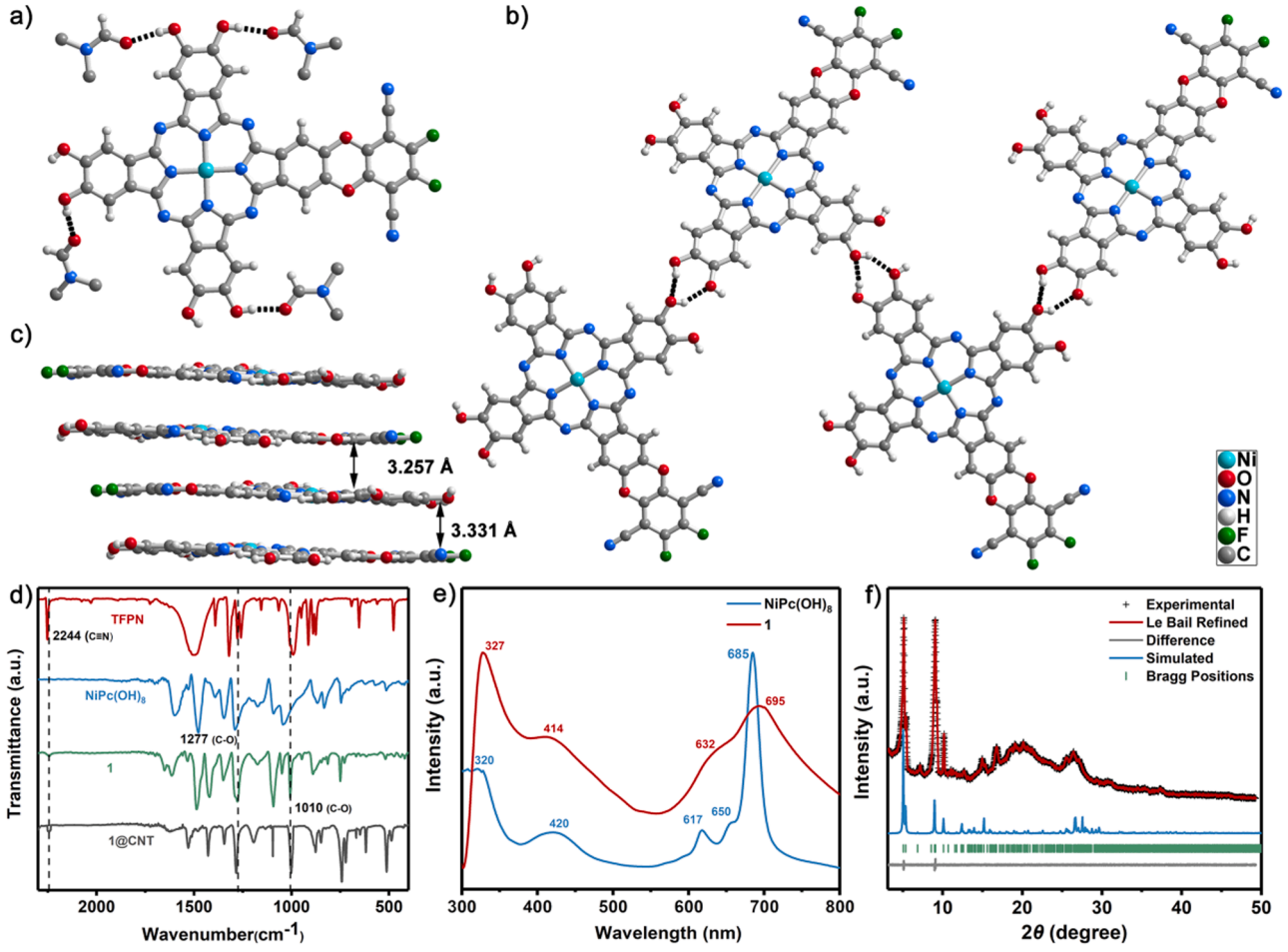

Fig. 1. (a) Crystal structure of an A3B-type asymmetric NiPc(OH)6(DCNFO) molecule and neighboring four DMF molecules with hydrogen bonding connection in 1; (b) Hydrogen bonding interactions between adjacent NiPc(OH)6(DCNFO) molecules in 1; (c) π-π interactions in 1; (d) Comparison in FT-IR spectra of 1, NiPc(OH)8, TFPN, and 1@CNT; (e) Comparison in UV–vis absorption of NiPc(OH)8 and 1; (f) PXRD characterization of 1: experimental PXRD profile (black), refined profile (red), difference (gray), and simulation pattern (cyan).

solubility in DMF (Fig. S2). After soaking **1** in organic solvents for one day, the unchanged crystal structure was confirmed by the consistent PXRD patterns with that of as-prepared species (Fig. S2), indicating the fact that this supramolecular structure possesses good solvent resistance, comparable with MOFs but different from molecular phthalocyanines. As a result, **1** should be a good heterogeneous catalyst for useful reactions. In addition, **1** shows good thermostability with the decomposed temperature higher than 400 °C (Fig. S3).

3.3. *In-situ preparation and characterization of 1@CNT*

The aggregating and poor conducting nature of molecule-based catalysts, whatever for metal complexes and polymeric materials, requires the necessary immobilization with conductive substrates. CNTs have unique electrical conductivity, high thermal stability and intrinsic mobility, as well as a high surface area that provides large specific surface area and rapid electron transfer. It can anchor molecular catalyst through physical adsorption and other forces [24]. As a result, **1** was doped on multiwalled CNTs using an in-situ preparation mode under the above-mentioned solvothermal reaction, giving the composites **1**@CNT (n) (n wt% = 7.8, 14.5, 22.1, and 29.8 wt% for the mass percentage of **1** in the composites, respectively). **1**@CNT(22.1) as a representative of this series of composites was carefully characterized. The FT-IR spectrum of **1**@CNT(22.1) displays the bands at 2244, 1319, and 1010 cm^{-1} (Fig. 1d), indicating the attendance of **1** in this composite. On the other hand, the Q band of **1**@CNT(22.1) was slightly shifted to 699 nm as compared with that of the pristine $NiPc(OH)_6$(DCNFO) (695 nm) (Fig. S4), suggesting the presence of the interface interaction between $NiPc(OH)_6$(DCNFO) and CNTs. Nevertheless, the high resolution mass spectrometry (HRMS) data show only two ionic fragment m/s signals at 671.09 and 856.95 (Fig. S5), exactly corresponding to the molecular formula $[M - 2\,H]^+$ and $[M - C_8F_2N_2O_2 + 6\,H]^+$ (M = 859.3) for NiPc $(OH)_6$(DCNFO). This evidence indicates the in-situ immobilization of **1** component on CNTs (Fig. S5).

One-dimensional fiber-like morphology of **1**@CNT(22.1) was clearly captured by scanning electron microscope (SEM) photo, Fig. S6 (Supplementary Material). In contrast to the naked CNTs, the thicken diameter of **1**@CNT(22.1) shown in transmission electron microscope (TEM) photo suggests the successful immobilization by addition of CNTs into the solvothermal reaction (Fig. 2a and b). In addition, TEM and aberration corrected high angle annular dark-field scanning transmission electron microscopy (AC HAADF-STEM) photos clearly disclose that CNTs (in dark color) were intimately covered by thin-layered **1** with the thickness of 2–4 nm (Figs. 2b, c and S7). **1**@CNT(22.1) has none PXRD diffraction of supramolecular compound due possibly to the low mass content of **1** in this composite. Such a hypothesis is supported by a typical diffraction signal of **1** at 5.1° on the composite with the increased mass content of phthalocyanine compound up to 75.0 wt% (Fig. S8). Energy dispersive X-ray spectroscopy (EDX) element mapping observes C, N, F, and Ni elements (Fig. S9), determining successful immobilization of **1** on CNTs. Comparative studies of the electronic structure of $NiPc(OH)_6$(DCNFO) in **1** and **1**@CNT were carried out on X-ray photoelectron spectroscopy (XPS) (Fig. 2d). In **1**, the binding energy of Ni $2p_{3/2}$ peak appears at 855.4 eV. After the deposition of **1** on CNTs, a slight shift of Ni $2p_{3/2}$ peak moves to 855.7 eV in the XPS spectrum of **1**@CNT, suggesting the strong π-π interactions between metallic phthalocyanine macrocycle and CNTs surface. Extended X-ray absorption fine structure (EXAFS) spectrum of the Ni K-edge for **1**@CNT(22.1) is similar to that of **1** (Fig. 2e and S10, Table S4), manifesting their similar Ni coordination geometries. It is worth noting that there is a slightly negative shift for a second intense peak at 8335.84 eV, which originates from the characteristic transition for Ni–N_4 coordination interactions, in the Ni K-edge X-ray absorption near-edge spectra (XANES) of **1**@CNT(22.1) relative to that of **1** (Fig. 2f). This evidence further discloses the presence of π-π interactions between **1** and CNTs [61,62,80,81].

3.4. *Electrocatalytic CO_2RR in H-type cell*

The electrocatalytic performances of **1**@CNT(n) (n = 7.8, 14.5, 22.1, and 29.8) in the H-type cell were investigated in comparison with that of **1**&CNT, **1**&CB (CB: conductive black) under the same conditions. **1**&CNT and **1**&CB were made by grinding the mixtures of **1** and different

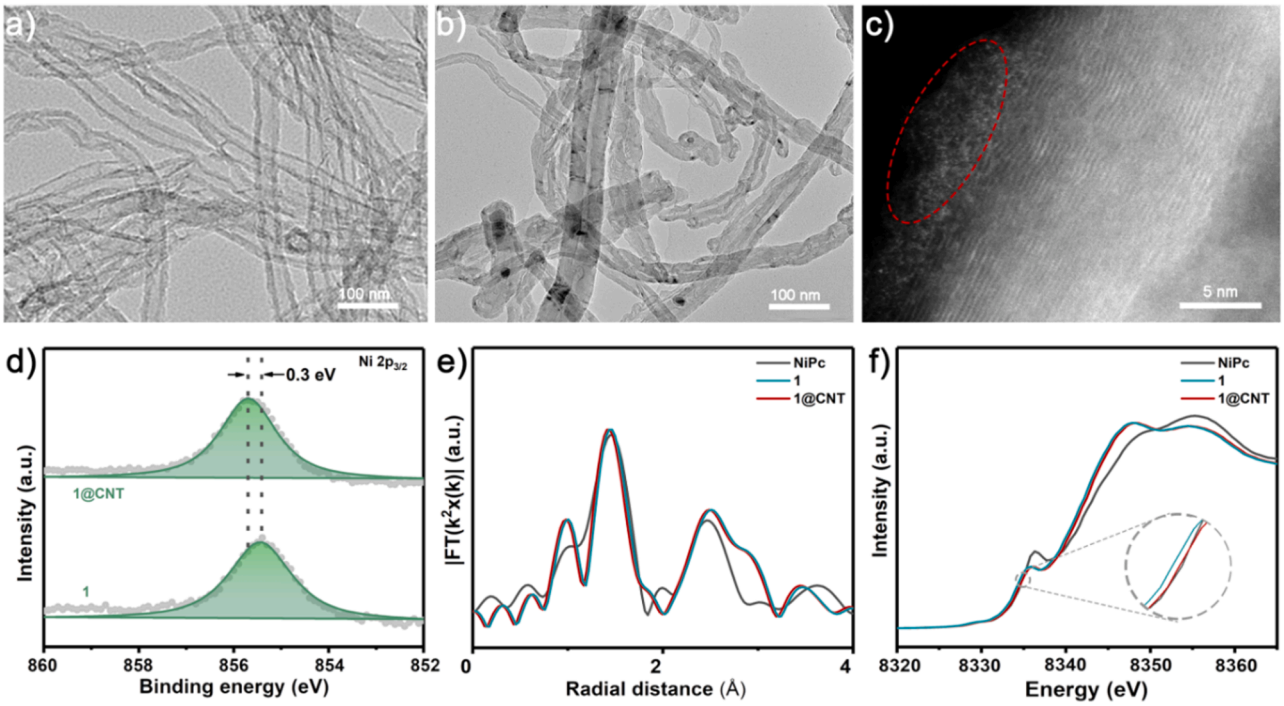

Fig. 2. (a) TEM image of CNTs; (b) TEM image of **1**@CNT(22.1); (c) AC HAADF-STEM photo of **1**@CNT(22.1); (d) Ni $2p_{3/2}$ XPS spectra of **1** and **1**@CNT(22.1); (e) Experimental curves of unsubstituted phthalocyanine (NiPc), **1**, and **1**@CNT; (f) Ni K-edge of XANES spectra of NiPc, **1**, and **1**@CNT.

conductive substances, respectively. The weight percentage of 22.1 wt% for **1** in **1**&CNT and **1**&CB was selected due to **1**@CNT(22.1) with the same active catalyst weight percentage showing the most excellent electrochemical catalytic activity among four *in-situ* prepared composites. The reference $NiPc(OH)_8$ @CNT was also prepared by adding CNTs into the solvothermal solution containing only $NiPc(OH)_8$. Gas chromatographic (GC) and liquid ^1H NMR spectroscopic results disclose the presence of only binary gas products including carbon monoxide (CO) and hydrogen (H_2) (Figs. S11 and S12). All mentioned potentials below were converted to the values versus RHE. **1**@CNT(22.1) electrode in Ar-saturated 0.5 M $KHCO_3$ electrolyte shows the very slow increase of current density along with the potential changing from 0 to 1.0 V in the linear sweep voltammetry (LSV) curve (Fig. 3a). In contrast, the replacement of Ar-saturated electrolyte with CO_2-saturated species leads to the surge of current density, suggesting efficient CO_2 catalysis on **1**@CNT(22.1). Moreover, LSV curves in CO_2-saturated 0.5 M $KHCO_3$ electrolyte reveals that **1**@CNT(22.1) presents a lower onset potential (–0.44 V, where the reduction current density reaches 0.1 mA cm^{-2}) and a larger total current density (68.3 mA cm^{-2}) at −1.0 V compared to the others with different loading amounts, Fig. S13. The optimal weight percentage of **1** on composite was thus identified as 22.1 wt%. Nevertheless, the onset potential of − 0.44 V for **1**@CNT(22.1) is a bit positive than those for the controls including **1**&CNT (−0.47 V), **1**&CB (−0.49 V), and $NiPc(OH)_8$ @CNT (−0.48 V), confirming the catalytic activity and advantages of in-situ growth of **1** on CNTs. Such tendency was also monitored in their CO partial current densities (j_{CO}) at the potential range of − 0.5 to − 1.1 V (Figs. 3b and S14). In particular, **1**@CNT(22.1) possesses an exceptional selectivity towards CO (FE_{CO} > 98%) with a current density of 12.2 mA cm^{-2} at − 0.7 V and 55.1 mA cm^{-2} at − 1.1 V, much higher than those of **1**&CNT (6.6 mA cm^{-2} at −0.7 V and 25.8 mA cm^{-2} at −1.1 V), **1**&CB (1.8 mA cm^{-2} at −0.7 V and 20.8 mA cm^{-2} at −1.1 V), and $NiPc(OH)_8$ @CNT (1.8 mA cm^{-2} at −0.7 V and 24.1 mA cm^{-2} at −1.1 V) (Fig. 3b). Meanwhile, the FE_{CO} of **1**@CNT(22.1) maintains a level of above 98% in the potential range from − 0.7∼− 1.1 V, Fig. 3c, demonstrating an enhanced selectivity of CO for CO_2RR in comparison with **1**&CNT, **1**&CB, and $NiPc(OH)_8$ @CNT. These results further evidence the material advantages of **1**@CNT(22.1) in electrocatalysis. The nickel content of **1**@CNT(22.1) amounts to ca. 1.0 wt% based on ICP-AES test (Table S5). As a result, the TOF is calculated as 3.3 s^{-1} at − 1.1 V, higher than those of all thus far reported nickel phthalocyanine-based polymeric electrocatalysts [45,46,75,78] and some nickel-based single-atom catalysts (SACs) [82–87], (Fig. 3d and Table S6). It is worth noting that j_{CO} of **1**@CNT(22.1) with current density of − 49 mA cm^{-2} at − 1.0 V is much bigger than those of most state-of-the-art molecule-based electrodes with polymeric structures such as NiPc-NiO_4 (24 mA cm^{-2} at −1.0 V) [75] and NiPc-TFPNCOF (15 mA cm^{-2} at −1.0 V) [46] under the similar operation conditions, revealing the excellent catalytic activity of **1**@CNT(22.1) (Fig. 3e).

Tafel slope of 75 mV dec^{-1} for **1**@CNT(22.1) is much smaller than those for **1**&CNT (94 mV dec^{-1}) and **1**&CB (113 mV dec^{-1}), demonstrating its faster dynamic process towards the electrochemical CO_2RR due to the thin-layered dispersion of **1** on CNTs prepared by the in-situ preparation method (Fig. S16). In addition, electrochemical impedance spectroscopy (EIS) data reveal that the charge transfer resistances of the composite electrocatalysts rank in the order of **1**@CNT(22.1) < **1**&CNT < **1**&CB (Fig. S17). The smaller resistance for **1**@CNT(22.1) is beneficial to the efficient charge transfer from conductive substrates to metal phthalocyanine electrocatalyst. **1**@CNT(22.1) also displays considerable electrochemical stability, as indicated by the retained 98% initial j_{CO} with constant FE_{CO} of 98% after 10 h cycling operation at − 0.9 V (Fig. 3f).

3.5. Electrocatalytic CO_2RR in flow cell

A series of above-mentioned electrocatalysts including **1**@CNT(n), **1**&CNT, **1**&CB, and $NiPc(OH)_8$ @CNT electrodes were installed as gas diffusion electrode on a flow cell as the CO_2RR electrolyzer (please see Fig. S19 in Supplementary Material for the device principle figure and methods for details). In 0.5 M $KHCO_3$ electrolyte, the current densities for these electrodes in flow cell are much superior to corresponding values determined in H-type cell. As shown in Fig. 4a, **1**@CNT(22.1)

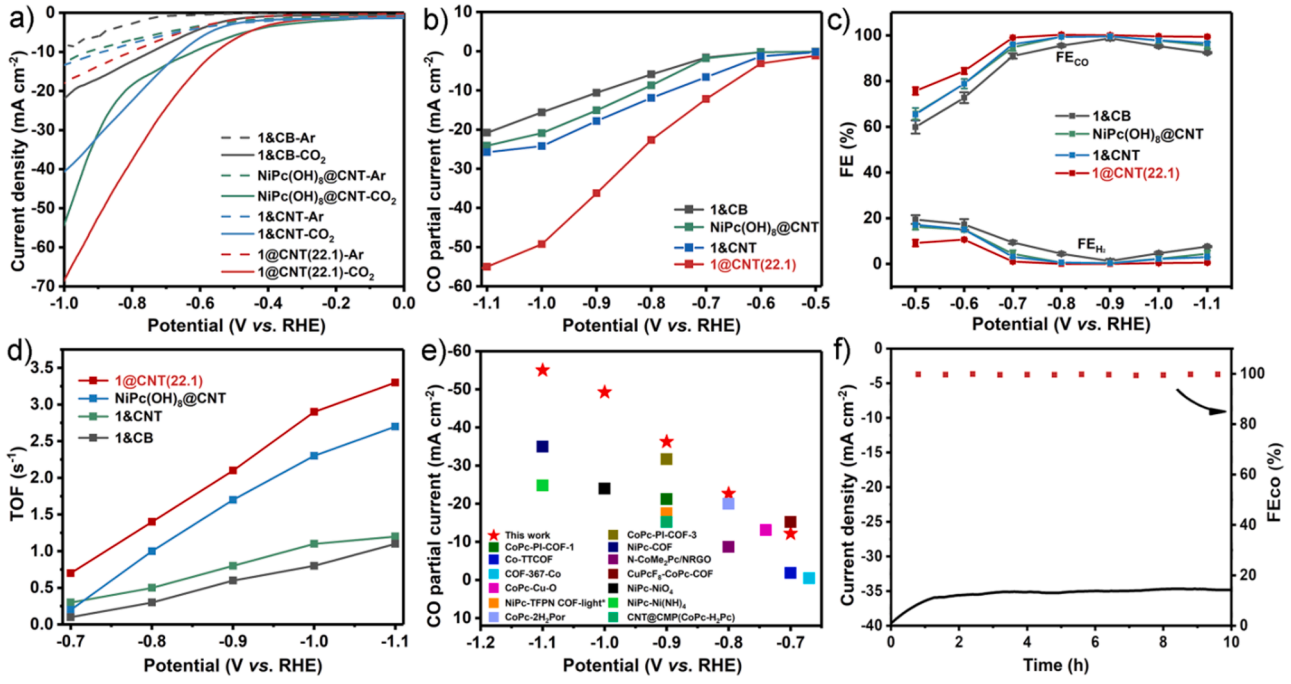

Fig. 3. (a) LSV profiles of **1**@CNT(22.1), **1**&CB, $NiPc(OH)_8$@CNT, and **1**&CNT in Ar- and CO_2-saturated 0.5 M $KHCO_3$ electrolytes at a scan rate of 10 mV s^{-1}; (b) Current densities of **1**@CNT(22.1), **1**&CB, $NiPc(OH)_8$@CNT, and **1**&CNT at different potentials in 0.5 M $KHCO_3$ electrolyte; (c) FE_{CO} and FE_{H2} of **1**@CNT(22.1), **1**&CB, $NiPc(OH)_8$@CNT, and **1**&CNT in a H-type cell; (d) TOF of **1**@CNT(22.1), **1**&CB, $NiPc(OH)_8$@CNT, and **1**&CNT in a H-type cell; (e) Comparison of j_{CO} of **1**@CNT(22.1) electrocatalyst performed in H-type electrochemical cell; (f) Stability of **1**@CNT at a potential of −0.9 V versus RHE in a H-type cell.

possesses a current density of 145 and 312 mA cm^{-2} at − 0.9 and − 1.1 V, respectively, being 3.0- and 4.7-time larger than the corresponding values of 36 and 55 mA cm^{-2} measured in H-type cell. Such excellent electrochemical activity of **1**@CNT(22.1) is originated from fast CO_2 diffusion to active electrocatalyst in gas diffusion electrode [39]. In the flow cell upon the employment of these electrocatalysts, still only H_2 and CO were detected by GC. FE_{CO} of **1**@CNT(22.1) was able to be constantly kept above 98% at a whole current scope up to 353 mA cm^{-2} (Fig. 4a and b), representing one of the best electrocatalytic activities among the molecule-based supramolecular catalysts and outperforming many excellent covalent-linked materials including NiPc-COF [45], NiPcP [49], and NiPPc/CNT [51], and even comparable with those in other SACs, noble metal and molecule electrocatalysts [88–95], Table S7. In contrast, **1**&CNT, **1**&CB, and $NiPc(OH)_8$ @CNT exhibit the high FE_{CO} above 98% with a much narrower voltage ranges, Fig. 4b, further indicating the materials advantage of in-situ immobilization of supramolecular electrocatalysts on conductive substrate in electrocatalysis. Due to the intrinsic flooding issues of the flow cell, cycling test of **1**@CNT(22.1) was checked at the current of 150 mA cm^{-2} for 40 h (Fig. 4c). The slight decay of current density was detected with the FE_{CO} maintained above 98%, revealing the superior stability of this composite in electrochemical CO_2 conversion.

Interestingly, replacing 0.5 M $KHCO_3$ electrolyte by 1.0 M KOH in the flow cell led to an increased j_{CO} of **1**@CNT(22.1) to 620 mA cm^{-2} at − 1.2 V with a high FE_{CO} of 98% (Fig. S20). Subsequently, the constant-current electrolysis of **1**@CNT(22.1) at the current density of 230 mA cm^{-2} was performed. As shown in Fig. 4d, no significant increase in the applied potential is noticed during 40 h continuous test, further confirming the excellent durability of **1**@CNT(n) catalyst in this flow cell device. Herein, it is noteworthy that the present work reports the effective immobilization of molecule-based catalysts on the electrode by solvothermal formation of insoluble supramolecular polymer on conductive substrate through π-π interaction. It is different from the heterogeneous methodology through sole physical adsorption, covalent linking, and polymerization, but similar to that for organic frameworks materials [24]. In addition, this work is able to modify microenvironment of active site by simultaneous introduction of substituents and immobilization on carbon tubes, it also enhances the catalyst stability by forming a new supramolecular polymer.

4. Theoretical calculations

In order to rationalize the excellent electrocatalytic behavior of 1 @CNT(22.1), density functional theory (DFT) calculation for $NiPc(OH)_6$(DCNFO) was carried out. In comparison with $NiPc(OH)_8$, $NiPc(OH)_6$(DCNFO) has a broader conjugating structure constructed by the covalent fusion of two aromatic systems of $NiPc(OH)_6$ and DCNFO. As shown in Figs. S21 and S22, the π electron localized orbital locator (π-LOL) calculation data clearly show the bigger conjugating system for $NiPc(OH)_6$(DCNFO) relative to that of $NiPc(OH)_8$. The large conjugating system of $NiPc(OH)_6$(DCNFO) leads to a narrow HOMO-LUMO gap, which benefits to the electron transmission in the present molecular material [96], and thus the catalyzing activity. It is worth noting that charge differential density of $NiPc(OH)_6$(DCNFO)@C (representing a $NiPc(OH)_6$(DCNFO) molecule located on graphite segment instead of 1 @CNT) also was explored according to DFT calculations toward understanding the interaction between $NiPc(OH)_6$(DCNFO) and CNTs in the electrocatalyst. As shown in Fig. S23, observation of strong inter-layered π-π interactions between $NiPc(OH)_6$(DCNFO) and carbon interface is consistent with the previous XPS test results, facilitating the rapid electron transport in the composite electrode [97–99].

The electron density difference (EDD) result proves that the electron

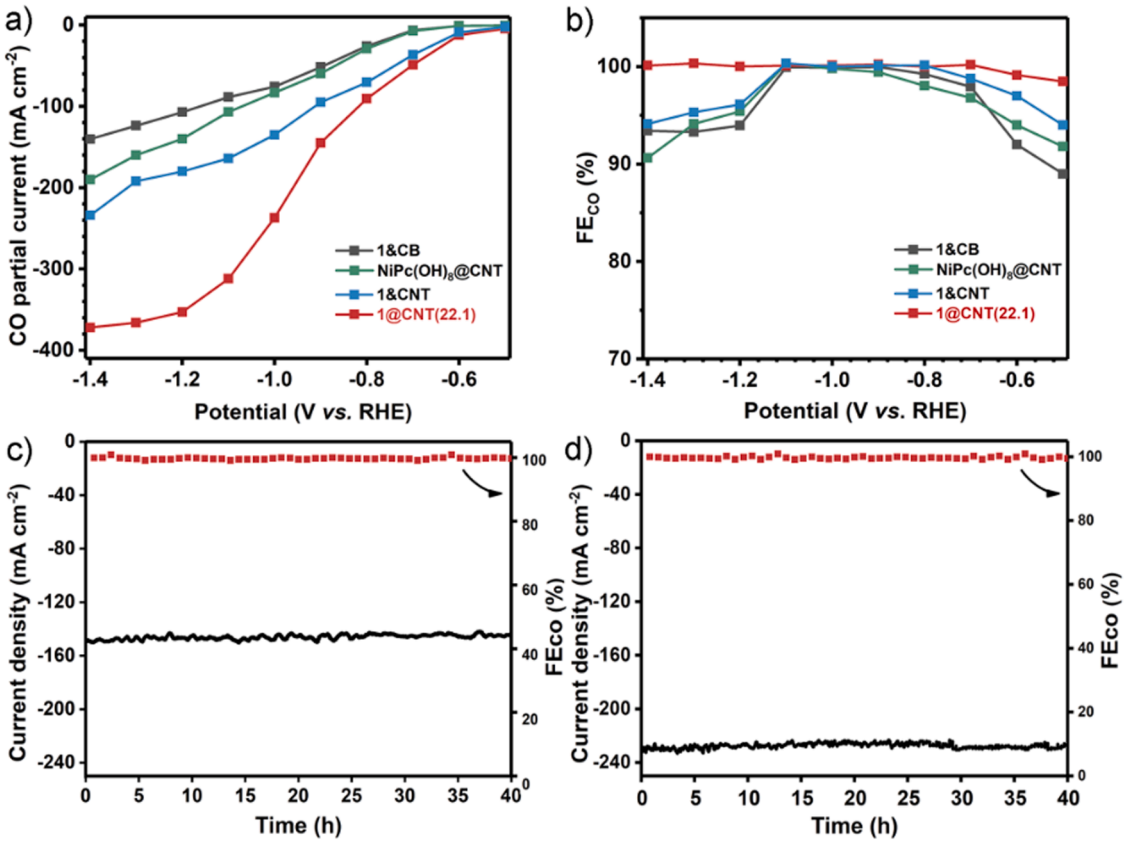

Fig. 4. (a) Current densities of **1**&CB, $NiPc(OH)_8$@CNT, **1**&CNT and **1**@CNT(22.1) at different potentials in a flow cell with 0.5 M $KHCO_3$ electrolyte; (b) FE_{CO} of **1**&CB, $NiPc(OH)_8$@CNT, **1**&CNT and **1**@CNT(22.1) in a flow cell with 0.5 M $KHCO_3$ electrolyte; (c) Stability of **1**@CNT(22.1) at 150 mA cm^{-2} in a flow cell with 0.5 M $KHCO_3$ electrolyte; (d) Stability of **1**@CNT(22.1) at 230 mA cm^{-2} in a flow cell with 1.0 M KOH electrolyte.

density is crowded around the Ni atom of metallic phthalocyanines (Fig. 4a). In addition, a charge density calculation further proves that the electron density of + 2.049 e Å^{-3} for Ni atom in NiPc(OH)$_6$(DCNFO), higher than that in NiPc(OH)$_8$ (+2.040 e Å^{-3}) and NiPc (+2.032 e Å^{-3}). This result is in good agreement with the Ni K-edge XANES data. The higher electron concentration around the Ni atom should be helpful to absorb the CO_2 molecule (Figs. 5a, 5b and S24). In addition, the Gibbs free energy diagram for the CO_2RR pathways was also calculated on NiPc(OH)$_6$(DCNFO), NiPc(OH)$_8$, and NiPc, respectively (Fig. 5e). According to the calculated electrochemical reducing diagram for the CO_2→CO conversion, a standard proton-coupled electron transfer (PCET), $* + CO_2 + H^+ + e^- \rightarrow *COOH$, takes place initially as the rate-determining step (R.D.S.) for all the three model catalysts [100,101]. Among the present three model catalysts, NiPc(OH)$_6$(DCNFO) has the lowest energy barrier of 0.62 eV, indicating its highest catalyzing efficiency.

The molecular structural calculation on the X-[NiY] complexes [X = CO_2 or CO; Y = Pc(OH)$_6$(DCNFO), Pc(OH)$_8$, or Pc] also provides useful information to understand the excellent catalyzing efficiency of Pc(OH)$_6$(DCNFO). Before the reaction, the distance between CO_2 carbon atom and Ni atom of molecular electrocatalyst is 2.87, 2.95, and 3.02 Å for NiPc(OH)$_6$(DCNFO), NiPc(OH)$_8$, and NiPc, respectively, indicating the strongest interaction between CO_2 and the former compound. For the desorption process of electrocatalytic CO_2RR, the distance between CO carbon atom and Ni atom from electrocatalyst is 2.84, 2.82, and 2.81 Å for NiPc(OH)$_6$(DCNFO), NiPc(OH)$_8$, and NiPc, respectively, suggesting the weakest attraction between CO and NiPc(OH)$_6$(DCNFO) (Fig. S25). As a result, the strongest CO_2 adsorption and CO desorption abilities of NiPc(OH)$_6$(DCNFO) among three species are helpful for corresponding CO_2RR electrocatalysis.

5. Conclusion

In summary, a supramolecular structure based a new A_3B-type asymmetric phthalocyanine nickel molecule directly prepared by the solvothermal reaction has been introduced, displaying the comparable solvent resistance to MOFs. This supramolecular structure has been used as a molecule-based polymeric electrocatalyst, rather than a dispersed molecular sample, towards carbon dioxide reduction reaction. In comparison with control electrodes made up of different molecular catalyst and various conductive substrates prepared by mechanical grinding, a composite generated by in-situ growth of this compound on carbon tubes exhibits superior electrocatalytic activities to selectively convert CO_2 to CO under industry-compatible current densities. The excellent electrocatalytic activity of this composite electrode has been well correlated from both experimental and theoretical perspectives. The present work not only provides a new excellent molecule-based polymeric electrocatalyst to provide industry-compatible current density and excellent selectivity, but also could give a clear hint that the electrocatalytic activities of MOFs and COFs electrodes reported previously might be further improved by using a suitable fabrication method to disperse active materials on conductive substrates.

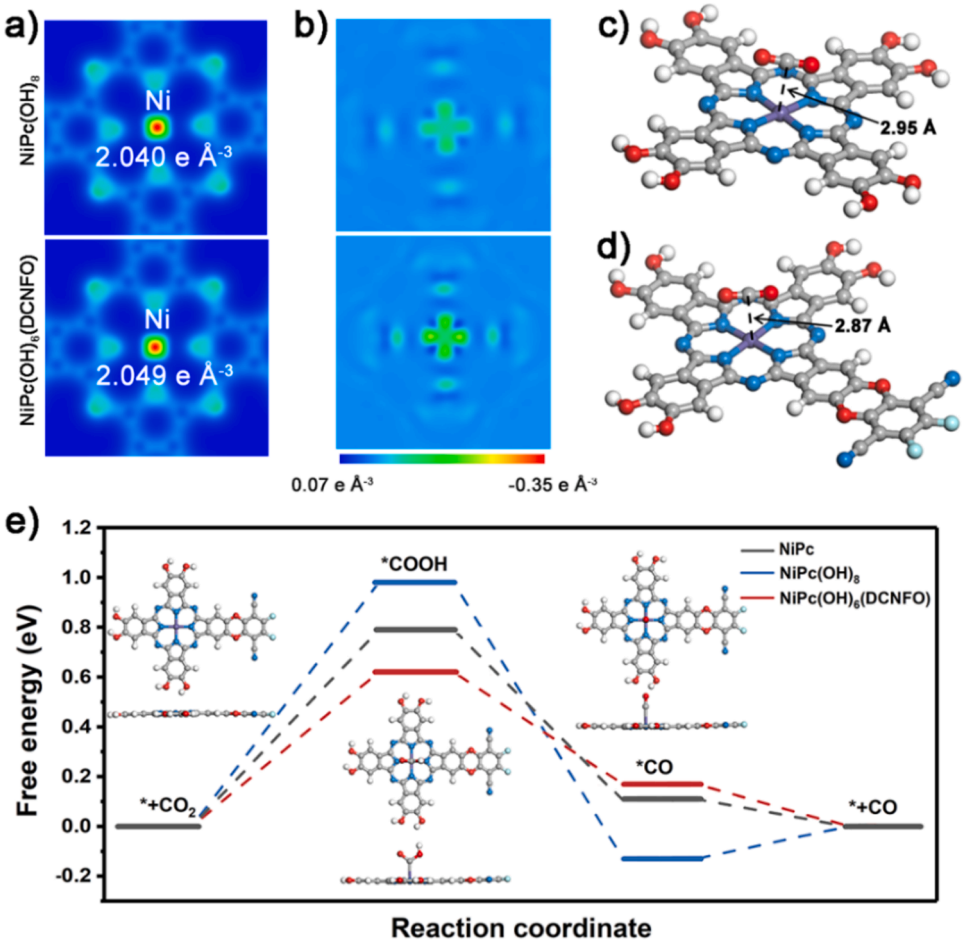

Fig. 5. (a) Charge density differences (the cyan and orange indicate electron accumulation and depletion) of NiPc(OH)$_8$ and NiPc(OH)$_6$(DCNFO); (b) Electron densities of NiPc(OH)$_8$ and NiPc(OH)$_6$(DCNFO); (c, d) Molecular structures of CO_2-adsorbed NiPc(OH)$_8$ and NiPc(OH)$_6$(DCNFO); (e) Free energy diagrams of NiPc (OH)$_8$ and NiPc(OH)$_6$(DCNFO) for CO_2RR (inset: molecular structure of NiPc(OH)$_6$(DCNFO) in CO_2RR process).

CRediT authorship contribution statement

Y.J. and Y.Z, conceived the project and designed the experiments. X. Z. and H.W. fabricated the electrocatalytic measurements and analysed the data. X.L. and B.Y. performed SEM and TEM characterizations. X.D. and T.Z. performed theoretical computations. Y.J. and H.W. wrote the manuscript. K.W., D.Q. and J.J. supervised the work and polished the manuscript.

Declaration of Competing Interest

The authors declare that they have no known competing financial interests or personal relationships that could have appeared to influence the work reported in this paper.

Data availability

Data will be made available on request.

Acknowledgments

This work was financially supported by the Natural Science Foundation of China (Nos. 22235001, 22131005, 22011540002, 22175020, 21871024, and 21631003), Xiaomi Young Scholar Programme, the Fundamental Research Funds for the Central Universities, and University of Science and Technology Beijing.

Appendix A. Supplementary material

Supplementary data associated with this article can be found in the online version at doi:10.1016/j.apcatb.2023.122446.

References

[1] T. Schwander, L. Schada von Borzyskowski, S. Burgener, N.S. Cortina, T.J. Erb, A synthetic pathway for the fixation of carbon dioxide in vitro, Science 354 (2016) 900.
[2] J. Artz, T.E. Müller, K. Thenert, Sustainable conversion of carbon dioxide: an integrated review of catalysis and life cycle assessment, Chem. Rev. 118 (2018) 434–504.
[3] J. Li, H. Huang, W. Xue, K. Sun, X. Song, C. Wu, L. Nie, Y. Li, C. Liu, Y. Pan, H.-L. Jiang, D. Mei, C. Zhong, Self-adaptive dual-metal-site pairs in metal-organic frameworks for selective CO_2 photoreduction to CH_4, Nat. Catal. 4 (2021) 719–729.
[4] H. Rao, L.C. Schmidt, J. Bonin, M. Robert, Visible-light-driven methane formation from CO_2 with a molecular iron catalyst, Nature 548 (2017) 74–77.
[5] X. Jiang, X. Nie, X. Guo, C. Song, J.G. Chen, Recent advances in carbon dioxide hydrogenation to methanol via heterogeneous catalysis, Chem. Rev. 120 (2020) 7984–8034.
[6] W. Liu, X. Li, C. Wang, H. Pan, W. Liu, K. Wang, Q. Zeng, R. Wang, J. Jiang, A scalable general synthetic approach toward ultrathin imine-linked two-dimensional covalent organic framework nanosheets for photocatalytic CO_2 reduction, J. Am. Chem. Soc. 141 (2019) 17431–17440.
[7] Z. Liang, C. Qu, D. Xia, R. Zou, Q. Xu, Atomically dispersed metal sites in MOF-based materials for electrocatalytic and photocatalytic energy conversion, Angew. Chem. Int. Ed. 57 (2018) 9604–9633. Angew. Chem. 130 (2018) 9750-9780.
[8] A. Kumar, V.K. Vashistha, D.K. Das, Recent development on metal phthalocyanines based materials for energy conversion and storage applications, Coord. Chem. Rev. 431 (2020), 213678.
[9] Q. Song, Z. Zhou, L. He, Efficient, selective and sustainable catalysis of carbon dioxide, Green Chem. 19 (2017) 3707.
[10] C.-T. Dinh, T. Burdyny, M.G. Kibria, A. Seifitokaldani, C.M. Gabardo, F.P. Garcia de Arquer, A. Kiani, J.P. Edwards, P. De Luna, O.S. Bushuyev, C. Zou, R. Quintero-Bermudez, Y. Pang, D. Sinton, E.H. Sargent, CO_2 electroreduction to ethylene via hydroxide-mediated copper catalysis at an abrupt interface, Science 360 (2018) 783–787.
[11] S. Gao, Y. Lin, X. Jiao, Y. Sun, Q. Luo, W. Zhang, D. Li, J. Yang, Y. Xie, Partially oxidized atomic cobalt layers for carbon dioxide electroreduction to liquid fuel, Nature 529 (2016) 68–71.
[12] G. Wang, J. Chen, Y. Ding, P. Cai, L. Yi, Y. Li, C. Tu, Y. Hou, Z. Wen, L. Dai, Electrocatalysis for CO_2 conversion: from fundamentals to value-added products, Chem. Soc. Rev. 50 (2021) 4993–5061.
[13] C.S. Diercks, Y.Z. Liu, K.E. Cordova, O.M. Yaghi, The role of reticular chemistry in the design of CO_2 reduction catalysts, Nat. Mater. 17 (2018) 301–307.
[14] K.E. Dalle, J. Warnan, J.J. Leung, B. Reuillard, I.S. Karmel, E. Reisner, Electro- and solar-driven fuel synthesis with first row transition metal complexes, Chem. Rev. 119 (2019) 2752–2875.
[15] R. Francke, B. Schille, M. Roemelt, Homogeneously catalyzed electroreduction of carbon dioxide—methods, mechanisms, and catalysts, Chem. Rev. 118 (2018) 4631–4701.
[16] J. Wang, W. Liu, D. Zhong, T. Lu, Nickel complexes as molecular catalysts for water splitting and CO_2 reduction, Coord. Chem. Rev. 378 (2019) 237–261.
[17] E. Boutin, M. Robert, Molecular electrochemical reduction of CO_2 beyond two electrons, Trends Chem. 3 (2021) 359–372.
[18] B. Siritanaratkul, C. Eagle, A.J. Cowan, Manganese carbonyl complexes as selective electrocatalysts for CO_2 reduction in water and organic solvents, Acc. Chem. Res. 55 (2022) 955–965.
[19] N.W. Kinzel, C. Werlé, W. Leitner, Transition metal complexes as catalysts for the electroconversion of CO_2: an organometallic perspective, Angew. Chem. Int. Ed. 60 (2021) 11628–11686. Angew. Chem. 133 (2021) 11732-11792.
[20] D. Grammatico, A. Bagnall, L. Riccardi, M. Fontecave, B. Su, L. Billon, Heterogenised molecular catalysts for sustainable electrochemical CO_2 reduction, Angew. Chem. Int. Ed. 61 (2022), e202206399.
[21] Y. Wu, Y. Liang, H. Wang, Heterogeneous molecular catalysts of metal phthalocyanines for electrochemical CO_2 reduction reactions, Acc. Chem. Res. 54 (2021) 3149–3159.
[22] F. Franco, C. Rettenmaier, H.S. Jeon, B. Roldan Cuenya, Transition metal-based catalysts for the electrochemical CO_2 reduction: from atoms and molecules to nanostructured materials, Chem. Soc. Rev. 49 (2020) 6884–6946.
[23] B. Zhang, L. Sun, Artificial photosynthesis: opportunities and challenges of molecular catalysts, Chem. Soc. Rev. 48 (2019) 2216–2264.
[24] Z. Yang, J. Chen, L. Qiu, W. Xie, L. He, Molecular engineering of metal complexes for electrocatalytic carbon dioxide reduction: from adjustment of intrinsic activity to molecular immobilization, Angew. Chem. Int. Ed. 61 (2022), e202205301.
[25] P.T. Smith, E.M. Nichols, Z. Cao, C.J. Chang, Hybrid catalysts for artificial photosynthesis: merging approaches from molecular, materials, and biological catalysis, Acc. Chem. Res. 53 (2020) 575–587.
[26] Z. Liang, H.-Y. Wang, H. Zheng, W. Zhang, R. Cao, Porphyrin-based frameworks for oxygen electrocatalysis and catalytic reduction of carbon dioxide, Chem. Soc. Rev. 50 (2021) 2540–2581.
[27] S. Yang, Y. Yu, X. Gao, Z. Zhang, F. Wang, Recent advances in electrocatalysis with phthalocyanines, Chem. Soc. Rev. 50 (2021) 12985–13011.
[28] E. Nikoloudakis, I. López-Duarte, G. Charalambidis, K. Ladomenou, M. Ince, A. G. Coutsolelos, Porphyrins and phthalocyanines as biomimetic tools for photocatalytic H_2 production and CO_2 reduction, Chem. Soc. Rev. 51 (2022) 6965–7045.
[29] C. Costentin, S. Drouet, M. Robert, J.M. Saveant, A. Local, Proton source enhances CO_2 electroreduction to CO by a molecular Fe catalyst, Science 338 (2012) 90–94.
[30] S. Meshitsuka, M. Ichikawa, K. Tamaru, Electrocatalysis by metal phthalocyanines in the reduction of carbon dioxide, J. Chem. Soc. Chem. Commun. (1974) 158–159.
[31] C. Kaminsky, S. Weng, J. Wright, Y. Surendranath, Adsorbed cobalt porphyrins act like metal surfaces in electrocatalysis, Nat. Catal. 5 (2022) 430–442.
[32] M. Lu, M. Zhang, J. Liu, Y. Chen, J.-P. Liao, M.-Y. Yang, Y.-P. Cai, S.-L. Li, Y.-Q. Lan, Covalent organic framework based functional materials: important catalysts for efficient CO_2 utilization, Angew. Chem. Int. Ed. 61 (2022), e202200003.
[33] Y. Wu, Z. Jiang, X. Lu, Y. Liang, H. Wang, Domino electroreduction of CO_2 to methanol on a molecular catalyst, Nature 575 (2019) 639–642.
[34] S. Lin, C.S. Diercks, Y.B. Zhang, N. Kornienko, E.M. Nichols, Y. Zhao, A.R. Paris, D. Kim, P. Yang, O.M. Yaghi, C.J. Chang, Covalent organic frameworks comprising cobalt porphyrins for catalytic CO_2 reduction in water, Science 349 (2015) 1208–1213.
[35] P. Rassu, X. Ma, B. Wang, Engineering of catalytically active sites in photoactive metal–organic frameworks, Coord. Chem. Rev. 465 (2022), 214561.
[36] X.F. Qiu, H.L. Zhu, J.R. Huang, P.Q. Liao, X.M. Chen, Highly selective CO_2 electroreduction to C_2H_4 using a metal–organic framework with dual active sites, J. Am. Chem. Soc. 143 (2021) 7242–7246.
[37] H. Zhong, M. Ghorbani-Asl, K.H. Ly, J. Zhang, J. Ge, M. Wang, Z. Liao, D. Makarov, E. Zschech, E. Brunner, I.M. Weidinger, J. Zhang, A. V. Krasheninnikov, S. Kaskel, R. Dong, X. Feng, Synergistic electroreduction of carbon dioxide to carbon monoxide on bimetallic layered conjugated metal-organic frameworks, Nat. Commun. 11 (2020) 1409–1418.
[38] M. Fang, L. Xu, H. Zhang, Y. Zhu, W. Wong, Metalloporphyrin-linked mercurated graphynes for ultrastable CO_2 electroreduction to CO with nearly 100% selectivity at a current density of 1.2 A cm–2, J. Am. Chem. Soc. 144 (2022) 15143–15154.
[39] S. Ren, D. Joulié, D. Salvatore, K. Torbensen, M. Wang, M. Robert, P. Berlinguette Curtis, Molecular electrocatalysts can mediate fast, selective CO_2 reduction in a flow cell, Science 365 (2019) 367–369.
[40] Z. Zhang, J. Xiao, X.-J. Chen, S. Yu, L. Yu, R. Si, Y. Wang, S. Wang, X. Meng, Y. Wang, Z.-Q. Tian, D. Deng, Reaction mechanisms of well-defined metal–N_4 sites in electrocatalytic CO_2 reduction, Angew. Chem. Int. Ed. 57 (2018) 16339–16342. Angew. Chem. 130 (2018) 16577-16580.
[41] L. Lin, H. Li, C. Yan, H. Li, R. Si, M. Li, J. Xiao, G. Wang, X. Bao, Synergistic catalysis over iron-nitrogen sites anchored with cobalt phthalocyanine for efficient CO_2 electroreduction, Adv. Mater. 31 (2019) 1903470.
[42] H. Liu, J. Chu, Z. Yin, X. Cai, L. Zhuang, H. Deng, Covalent organic frameworks linked by amine bonding for concerted electrochemical reduction of CO_2, Chem 4 (2018) 1696–1709.

[43] N. Huang, K.H. Lee, Y. Yue, X. Xu, S. Irle, Q. Jiang, D. Jiang, A stable and conductive metallophthalocyanine framework for electrocatalytic carbon dioxide reduction in water, Angew. Chem. Int. Ed. 59 (2020) 16587–16593.

[44] J. Yuan, S. Chen, Y. Zhang, R. Li, J. Zhang, T. Peng, Structural regulation of coupled phthalocyanine–porphyrin covalent organic frameworks to highly active and selective electrocatalytic CO_2 reduction, Adv. Mater. 34 (2022) 2203139.

[45] M.-D. Zhang, D.-H. Si, J.-D. Yi, S.-S. Zhao, Y.-B. Huang, R. Cao, Conductive phthalocyanine-based covalent organic framework for highly efficient electroreduction of carbon dioxide, Small 16 (2020) 2005254.

[46] M. Lu, M. Zhang, C.G. Liu, J. Liu, L.J. Shang, M. Wang, J.N. Chang, S.L. Li, Y. Q. Lan, Stable dioxin-linked metallophthalocyanine covalent organic frameworks (COFs) as photo-coupled electrocatalysts for CO_2 reduction, Angew. Chem. Int. Ed. 60 (2021) 4864–4871. Angew. Chem. 133 (2021) 4914-4921.

[47] Y. Yue, P. Cai, K. Xu, H. Li, H. Chen, H.-C. Zhou, N. Huang, Stable bimetallic polyphthalocyanine covalent organic frameworks as superior electrocatalysts, J. Am. Chem. Soc. 143 (2021) 18052–18060.

[48] Z. Meng, J. Luo, W. Li, K.A. Mirica, Hierarchical tuning of the performance of electrochemical carbon dioxide reduction using conductive two-dimensional metallophthalocyanine based metal–organic frameworks, J. Am. Chem. Soc. 142 (2020) 21656–21669.

[49] S. Wei, H. Zou, W. Rong, F. Zhang, Y. Ji, L. L.e Duan, Conjugated nickel phthalocyanine polymer selectively catalyzes CO_2-to-CO conversion in a wide operating potential window, Appl. Catal. B 284 (2021), 119739.

[50] W.W. Kramer, C.C.L. McCrory, Polymer coordination promotes selective CO_2 reduction by cobalt phthalocyanine, Chem. Sci. 7 (2016) 2506–2515.

[51] K. Chen, M. Cao, G. Ni, S. Chen, H. Liao, L. Zhu, H. Li, J. Fu, J. Hu, E. Cortés, M. Liu, Nickel polyphthalocyanine with electronic localization at the nickel site for enhanced CO_2 reduction reaction, Appl. Catal. B 306 (2022), 121093.

[52] N.G. Yasri, T.A. Al-Attas, J. Hu, M.G. Kibria, Electropolymerized metal-protoporphyrin electrodes for selective electrochemical reduction of CO_2, Catal. Sci. Technol. 11 (2021) 1580–1589.

[53] J. Chen, J. Li, W. Liu, X. Ma, J. Xu, M. Zhu, Y.-F. Han, Facile synthesis of polymerized cobalt phthalocyanines for highly efficient CO_2 reduction, Green Chem. 21 (2019) 6056–6061.

[54] R. Wang, X. Wang, W. Weng, Y. Yao, P. Kidkhunthod, C. Wang, Y. Hou, J. Guo, Proton/electron donors enhancing electrocatalytic activity of supported conjugated microporous polymers for CO_2 reduction, Angew. Chem. Int. Ed. 61 (2022), e202115503.

[55] E. Boutin, M. Wang, J.C. Lin, M. Mesnage, D. Mendoza, B. Lassalle-Kaiser, C. Hahn, T.F. Jaramillo, M. Robert, Aqueous electrochemical reduction of carbon dioxide and carbon monoxide into methanol with cobalt phthalocyanine, Angew. Chem. Int. Ed. 58 (2019) (2019) 16172–16176. Angew. Chem. 131 (2019) 16318–16322.

[56] P. Li, X. Lu, Z. Wu, Y. Wu, R. Malpass-Evans, N.B. McKeown, X. Sun, H. Wang, Acid–base interaction enhancing oxygen tolerance in electrocatalytic carbon dioxide reduction, Angew. Chem. Int. Ed. 59 (2020) 10918–10923. Angew. Chem. 132 (2020) 11010-11015.

[57] N. Han, Y. Wang, L. Ma, J. Wen, J. Li, H. Zheng, K. Nie, X. Wang, F. Zhao, Y. Li, J. Fan, J. Zhong, T. Wu, D.J. Miller, J. Lu, S.-T. Lee, Y. Li, Supported cobalt polyphthalocyanine for high-performance electrocatalytic CO_2 reduction, Chem 3 (2017) 652–664.

[58] M.A. Bajada, S. Roy, J. Warnan, K. Abdiaziz, A. Wagner, M.M. Roessler, E. Reisner, A. Precious-Metal-Free, Hybrid electrolyzer for alcohol oxidation coupled to CO_2-to-syngas conversion, Angew. Chem. Int. Ed. 59 (2020) 15633–15641. Angew. Chem. 132 (2020) 15763-15771.

[59] X. Zhang, Y. Wang, M. Gu, M. Wang, Z. Zhang, W. Pan, Z. Jiang, H. Zheng, M. Lucero, H. Wang, G.E. Sterbinsky, Q. Ma, Y.-G. Wang, Z. Feng, J. Li, H. Dai, Y. Liang, Molecular engineering of dispersed nickel phthalocyanines on carbon nanotubes for selective CO_2 reduction, Nat. Energy 5 (2020) 684–692.

[60] S. Liu, H.B. Yang, S.F. Hung, J. Ding, W. Cai, L. Liu, J. Gao, X. Li, X. Ren, Z. Kuang, Y. Huang, T. Zhang, B. Liu, Elucidating the electrocatalytic CO_2 reduction reaction over a model single-atom nickel catalyst, Angew. Chem. Int. Ed. 59 (2020) 798–803. Angew. Chem. 132 (2020) 808-813.

[61] S. Han, M. Zhang, Z. Fu, L. Zheng, D. Ma, X. Wu, Q. Zhu, Enzyme-inspired microenvironment engineering of a single-molecular heterojunction for promoting concerted electrochemical CO_2 reduction, Adv. Mater. 34 (2022) 2202830.

[62] D.-D. Ma, S.-G. Han, C. Cao, W. Wei, X. Li, B. Chen, X.-T. Wu, Q.-L. Zhu, Bifunctional single-molecular heterojunction enables completely selective CO_2-to-CO conversion integrated with oxidative 3D nano-polymerization, Energy Environ. Sci. 14 (2021) 1544–1552.

[63] D.-D. Ma, S.-G. Han, C. Cao, X. Li, X.-T. Wu, Q.-L. Zhu, Remarkable electrocatalytic CO_2 reduction with ultrahigh CO/H_2 ratio over single-molecularly immobilized pyrrolidinonyl nickel phthalocyanine, Appl. Catal. B 264 (2020), 118530.

[64] J. Su, J.-J. Zhang, J. Chen, Y. Song, L. Huang, M. Zhu, B.I. Yakobson, B.Z. Tang, R. Ye, Building a stable cationic molecule/electrode interface for highly efficient and durable CO_2 reduction at an industrially relevant current, Energy Environ. Sci. 14 (2021) 483–492.

[65] Jofrey Jackson Masana, J. Xiao, H. Zhang, X. Lu, M. Qiu, Y. Yu, Nitrogen-rich carbon nitride inducing electron delocalization of Co-N4 site to enhance electrocatalytic carbon dioxide reduction, Appl. Catal. B 323 (2023), 122199.

[66] P.K. Sonkar, V. Ganesan, R. Gupta, D.K. Yadav, M. Yadav, Nickel phthalocyanine integrated graphene architecture as bifunctional electrocatalyst for CO_2 and O_2 reductions, J. Electroanal. Chem. 826 (2018) 1.

[67] C. Chen, X. Sun, D. Yang, L. Lu, H. Wu, L. Zheng, P. An, J. Zhang, B. Han, Enhanced CO_2 electroreduction via interaction of dangling S bonds and Co sites in cobalt phthalocyanine/$ZnIn_2S_4$ hybrids, Chem. Sci. 10 (2019) 1659–1663.

[68] M. Wang, K. Torbensen, D. Salvatore, S. Ren, D. Joulie, F. Dumoulin, D. Mendoza, B. Lassalle-Kaiser, U. Isci, C.P. Berlinguette, M. Robert, CO_2 electrochemical catalytic reduction with a highly active cobalt phthalocyanine, Nat. Commun. 10 (2019) 3602.

[69] M. Zhu, J. Chen, R. Guo, J. Xu, X. Fang, Y.-F. Han, Cobalt phthalocyanine coordinated to pyridine-functionalized carbon nanotubes with enhanced CO_2 electroreduction, Appl. Catal. B 251 (2019) 112–118.

[70] S. Roy, M. Miller, J. Warnan, J.J. Leung, C.D. Sahm, E. Reisner, Electrocatalytic and solar-driven reduction of aqueous CO_2 with molecular cobalt phthalocyanine–metal oxide hybrid materials, ACS Catal. 11 (2021) 1868–1876.

[71] Z. Meng, A. Aykanat, K.A. Mirica, Welding metallophthalocyanines into bimetallic molecular meshes for ultrasensitive, low-power chemiresistive detection of gases, J. Am. Chem. Soc. 141 (2015) 2046–2053.

[72] R. Matheu, E. Gutierrez-Puebla, M.A. Monge, C.S. Diercks, J. Kang, M.S. Prevot, X. Pei, N. Hanikel, B. Zhang, P. Yang, O.M. Yaghi, Three-dimensional phthalocyanine metal-catecholates for high electrochemical carbon dioxide reduction, J. Am. Chem. Soc. 141 (2019) 17081–17085.

[73] Y. Zhou, R. Abazari, J. Chen, M. Tahir, A. Kumar, R.R. Ikreedeegh, E. Rani, H. Singh, A.M. Kirillov, Bimetallic metal–organic frameworks and MOF-derived composites: recent progress on electro- and photoelectrocatalytic applications, Coord. Chem. Rev. 451 (2022), 214264.

[74] X. Qiu, J. Huang, C. Yu, Z. Zhao, H. Zhu, Z. Ke, P. Liao, X. Chen, A stable and conductive covalent organic framework with isolated active sites for highly selective electroreduction of carbon dioxide to acetate, Angew. Chem. Int. Ed. 61 (2022), e202206470.

[75] J.-D. Yi, D.-H. Si, R. Xie, Q. Yin, M.-D. Zhang, Q. Wu, G.-L. Chai, Y.-B. Huang, R. Cao, Conductive two-dimensional phthalocyanine-based metal–organic framework nanosheets for efficient electroreduction of CO_2, Angew. Chem. Int. Ed. 60 (2021) 17108–17114.

[76] B. Han, X. Ding, B. Yu, H. Wu, W. Zhou, W. Liu, C. Wei, B. Chen, D. Qi, H. Wang, K. Wang, Y. Chen, B. Chen, J. Jiang, Two-dimensional covalent organic frameworks with cobalt(II)-phthalocyanine sites for efficient electrocatalytic carbon dioxide reduction, J. Am. Chem. Soc. 143 (2021) 7104–7113.

[77] B. Han, Y. Jin, B. Chen, W. Zhou, B. Yu, C. Wei, H. Wang, K. Wang, Y. Chen, B. Chen, J. Jiang, Maximizing electroactive sites in a three-dimensional covalentorganic framework for significantly improved carbon dioxide reduction electrocatalysis, Angew. Chem. Int. Ed. 61 (2022), e202114244.

[78] M.-D. Zhang, D.-H. Si, J.-D. Yi, Q. Yin, Y.-B. Huang, R. Cao, Conductive phthalocyanine-based metal-organic framework as a highly efficient electrocatalyst for carbon dioxide reduction reaction, Sci. China Chem. 64 (2021) 1332–1339.

[79] H. Jiang, P. Hu, J. Ye, R. Ganguly, Y. Li, Y. Long, D. Fichou, W. Hu, C. Kloc, Hole mobility modulation in single-crystal metal phthalocyanines by changing the metal–π/π–π interactions, Angew. Chem. Int. Ed. 57 (2018) 10112–10117.

[80] J. Su, G.D. Li, X.H. Li, J.S. Chen, 2D/2D heterojunctions for catalysis, Adv. Sci. 6 (2019) 1801702.

[81] K.X. Zhang, H. Su, H.H. Wang, J.J. Zhang, S.Y. Zhao, W. Lei, X. Wei, X.H. Li, J. S. Chen, Atomic-scale Mott–Schottky heterojunctions of boron nitride monolayer and graphene as metal-free photocatalysts for artificial photosynthesis, Adv. Sci. 5 (2018) 1800062.

[82] C. Yan, H. Li, Y. Ye, H. Wu, F. Cai, R. Si, J. Xiao, S. Miao, S. Xie, F. Yang, Y. Li, G. Wang, X. Bao, Coordinatively unsaturated nickel–nitrogen sites towards selective and high-rate CO_2 electroreduction, Energy Environ. Sci. 11 (2018) 1204–1210.

[83] J. Yang, Z. Qiu, C. Zhao, W. Wei, W. Chen, Z. Li, Y. Qu, J. Dong, J. Luo, Z. Li, Y. Wu, In situ thermal atomization to convert supported nickel nanoparticles into surface-bound nickel single-atom catalysts, Angew. Chem. Int. Ed. 57 (2018) 14095–14100.

[84] C. Zhao, X. Dai, T. Yao, W. Chen, X. Wang, J. Wang, J. Yang, S. Wei, Y. Wu, Y. Li, Ionic exchange of metal–organic frameworks to access single nickel sites for efficient electroreduction of CO_2, J. Am. Chem. Soc. 139 (2017) 8078–8081.

[85] Y.N. Gong, L. Jiao, Y. Qian, C.Y. Pan, L. Zheng, X. Cai, B. Liu, S.H. Yu, H. Jiang, Regulating the coordination environment of MOF-templated single-atom nickel electrocatalysts for boosting CO_2 reduction, Angew. Chem. Int. Ed. 59 (2020) 2705–2709.

[86] Y. Zhang, L. Jiao, W. Yang, C. Xie, H. Jiang, Rational fabrication of low-coordinate single-atom Ni electrocatalysts by MOFs for highly selective CO_2 reduction, Angew. Chem. Int. Ed. 60 (2021) 7607–7611.

[87] X. Cao, L. Zhao, B. Wulan, D. Tan, Q. Chen, J. Ma, J. Zhang, Atomic bridging structure of nickel–nitrogen–carbon for highly efficient electrocatalytic reduction of CO_2, Angew. Chem. Int. Ed. 61 (2022), e202113918.

[88] Z. Chen, X. Zhang, W. Liu, M. Jiao, K. Mou, X. Zhang, L. Liu, Amination strategy to boost the CO_2 electroreduction current density of M–N/C single-atom catalysts to the industrial application level, Energy Environ. Sci. 14 (2021) 2349–2356.

[89] X. Wang, X. Sang, C.-L. Dong, S. Yao, L. Shuai, J. Lu, B. Yang, Z. Li, L. Lei, M. Qiu, L. Dai, Y. Hou, Proton capture strategy for enhancing electrochemical CO_2 reduction on atomically dispersed metal–nitrogen active sites, Angew. Chem. Int. Ed. 60 (2021) 11959–11965.

[90] W. Ren, X. Tan, X. Chen, G. Zhang, K. Zhao, W. Yang, C. Jia, Y. Zhao, S.C. Smith, C. Zhao, Confinement of ionic liquids at single-Ni-sites boost electroreduction of CO_2 in aqueous electrolytes, ACS Catal. 10 (2020) 13171–13178.

[91] X. Zhang, Y. Wang, M. Gu, M. Wang, Z. Zhang, W. Pan, Z. Jiang, H. Zheng, M. Lucero, H. Wang, G.E. Sterbinsky, Q. Ma, Y.-G. Wang, Z. Feng, J. Li, H. Dai,

Y. Liang, Molecular engineering of dispersed nickel phthalocyanines on carbon nanotubes for selective CO_2 reduction, Nat. Energy 5 (2020) 684–692.
[92] S. Han, M. Zhang, Z. Fu, L. Zheng, D. Ma, X. Wu, Q. Zhu, Enzyme-inspired microenvironment engineering of a single-molecular heterojunction for promoting concerted electrochemical CO_2 reduction, Adv. Mater. 34 (2022) 2202830.
[93] R. Shi, J. Guo, X. Zhang, G.I.N. Waterhouse, Z. Han, Y. Zhao, L. Shang, C. Zhou, L. Jiang, T. Zhang, Efficient wettability-controlled electroreduction of CO_2 to CO at Au/C interfaces, Nat. Commun. 11 (2020) 3028.
[94] C.F. Wen, F. Mao, Y. Liu, X.Y. Zhang, H.Q. Fu, L.R. Zheng, P.F. Liu, H.G. Yang, Nitrogen-stabilized low-valent Ni motifs for efficient CO_2 electrocatalysis, ACS Catal. 10 (2020) 1086–1093.
[95] J. Wang, J. Yu, M. Sun, L. Liao, Q. Zhang, L. Zhai, X. Zhou, L. Li, G. Wang, F. Meng, D. Shen, Z. Li, H. Bao, Y. Wang, J. Zhou, Y. Chen, W. Niu, B. Huang, L. Gu, C.S. Lee, Z. Fan, Surface molecular functionalization of unusual phase metal nanomaterials for highly efficient electrochemical carbon dioxide reduction under industry-relevant current density, Small 18 (2022) 2106766.
[96] Q. Wu, M. Mao, Q. Wu, J. Liang, Y. Huang, R. Cao, Construction of donor–acceptor heterojunctions in covalent organic framework for enhanced CO_2 electroreduction, Small 17 (2021) 2004933.
[97] F. Tournus, S. Latil, M.I. Heggie, J.C. Charlier, π-Stacking interaction between carbon nanotubes and organic molecules, Phys. Rev. B 72 (2005), 075431.
[98] R. Shi, L. Liu, Y. Lu, Y. Li, S. Zheng, Z. Yan, K. Zhang, J. Chen, In situ polymerized conjugated poly(pyrene-4,5,9,10-tetraone)/carbon nanotubes composites for high-performance cathode of sodium batteries, Adv. Energy Mater. 11 (2021) 2002917.
[99] X. Liu, Y. Jin, H. Wang, X. Yang, P. Zhang, K. Wang, J. Jiang, In situ growth of covalent organic framework nanosheets on graphene as the cathode for long-life high-capacity lithium-ion batteries, Adv. Mater. (2022) 2203605.
[100] M. Ma, B.J. Trześniewski, J. Xie, W.A. Smith, Selective and efficient reduction of carbon dioxide to carbon monoxide on oxide-derived nanostructured silver electrocatalysts, Angew. Chem. Int. Ed. 55 (2016) 9748–9752.
[101] H.A. Hansen, J.B. Varley, A.A. Peterson, J.K. Nørskov, Understanding trends in the electrocatalytic activity of metals and enzymes for CO_2 reduction to CO, J. Phys. Chem. Lett. 4 (2013) 388–392.